July 1, 2013

Using Singlet Molecular Oxygen to Probe the Solute and Temperature Dependence of Liquid-Like Regions in/on Ice

Jonathan P. Bower[1] and Cort Anastasio[1,*]

[1]Department of Land, Air, and Water Resources
University of California, Davis
One Shields Avenue
Davis, CA 95616

*Corresponding author:

Cort Anastasio
Land, Air, and Water Resources
University of California, Davis
One Shields Avenue
Davis, CA
Telephone: 530.754.6095
Fax: 530.752.1552
email: canastasio@ucdavis.edu

Submitted to the Journal of Physical Chemistry A, April 24, 2013
Revision Submitted: July 10, 2013

Abstract

Liquid-like regions (LLRs) are found at the surfaces and grain boundaries of ice and as inclusions within ice. These regions contain most of the solutes in ice and can be (photo)chemically active hotspots in natural snow and ice systems. If we assume all solutes partition into LLRs as a solution freezes, freezing-point depression predicts that the concentration of a solute in LLRs is higher than its concentration in the pre-frozen (or melted) solution by the freeze-concentration factor (F). Here we use singlet molecular oxygen production to explore the effects of total solute concentration ([TS]) and temperature on experimentally determined values of F. For ice above its eutectic temperature, measured values of F agree well with freezing-point depression when [TS] is above ~1 mmol/kg; at lower [TS] values, measurements of F are lower than predicted from freezing-point depression. For ice below its eutectic temperature, the influence of freezing-point depression on F is damped; the extreme case is with Na_2SO_4 as the solute, where F shows essentially no agreement with freezing-point depression. In contrast, for ice containing 3 mmol/kg NaCl, measured values of F agree well with freezing-point depression over a range of temperatures, including below the eutectic. Our experiments also reveal that the photon flux in LLRs increases in the presence of salts, which has implications for ice photochemistry in the lab and, perhaps, in the environment.

Keywords

Ice kinetics, ice composition, quasi-liquid layer, freezing-point depression

Introduction

The presence of liquid-like (or quasi-liquid) layers on ice surfaces has been recognized for some time.[1] On pure water-ice, surface disorder occurs to minimize the energy at the ice-air or ice-substrate interface.[2] At temperatures very close to the melting point (–0.15˚C), this layer is indistinguishable from liquid water,[3] but at lower temperatures the thickness of the layer decreases and its physical properties become liquid-like rather than those of a true liquid.[4,5] Wei and coworkers found disorder in the surface layer on ice crystals grown from deionized water at temperatures as low as –73˚C; this disorder increased with temperature to the melting point at 0˚C.[6] Though their technique only probed the outermost monolayer of water molecules, they found the disordering of the surface monolayer was insensitive to the presence of impurities (e.g., salts)[6], suggesting neither the structure of the liquid-like region nor the distribution of solutes within them is necessarily homogeneous. Using a different technique, Donaldson and coworkers probed tens of monolayers of the liquid-like surface of a frozen salt solution and found evidence that it is a highly concentrated brine layer.[7] While these techniques all focused on the air-ice interface, liquid-like regions (LLRs) can also occur within an ice sample, for example as inclusions within ice crystals and at grain boundaries or triple junctions within the ice.

Two variables control the thickness (and thus volume) of these liquid-like regions in/on ice: the total concentration of solutes and temperature.[8] Using NMR, Cho and coworkers showed that the liquid-like water content of a frozen sample increases with increasing salt concentration and with increasing temperature.[9] Furthermore, above the eutectic temperature of the system, the solute and temperature dependence of the liquid-like regions closely matched the freezing-point depression (FPD) model,[9] which predicts

the composition of liquid-like regions in/on ice samples, assuming all solutes are excluded from the bulk ice into LLRs during freezing. In the freezing-point depression model, the (maximum) concentration of species "*m*" in liquid-like regions in/on ice (i.e., $[m]_{FPD,LLR}$) is related to its concentration in the unfrozen liquid solution ($[m]_{LIQ}$), the total solute concentration of the unfrozen solution ($[TS]_{LIQ}$), and the temperature (T, in K) of the frozen sample:

$$[m]_{FPD,LLR} = \frac{[m]_{LIQ}}{\varphi_{H2O}^{Max}(T)} \approx [m]_{LIQ} \left(\frac{|T - T_f|}{E_f [TS]_{LIQ}} \right) = [m]_{LIQ} F_{FPD} \quad (1)$$

In this equation, solute concentrations are in units of mol/kg-solvent, $\phi_{H2O}^{Max}(T)$ is the upper limit for the fraction of water molecules present in liquid-like regions of ice,[9] E_f is the cryoscopic constant (1.86 K kg/mol for water[10]), and F_{FPD} is the freeze-concentration factor based on freezing-point depression (i.e., $F_{FPD} = [m]_{FPD,LLR}/[m]_{LIQ}$). Based on Equation 1, reactions that depend on solute concentration should be enhanced in LLRs in/on ice relative to in the corresponding liquid solution. For example, for ice samples at –10˚C, the total concentration of solutes in LLRs is predicted to be 5.4 mol/kg, regardless of the solute concentration in the liquid prior to freezing (as long as the solution contained some solute). Thus if $[TS]_{LIQ}$ is 0.065 mmol/kg (a typical value in our low total solute solutions), the freezing-point depression model predicts that the concentration of each solute will increase by a factor of 8.3 10^4 when moving from solution to ice LLRs at –10˚C (i.e., $F_{FPD} = 8.3 \times 10^4$). However, the composition of LLRs is not necessarily simply a highly concentrated analogue of the starting solution; for example, there can be important differences in the pH of LLRs

compared to the initial solution because of preferential incorporation of ions into the growing ice.[11]

There is experimental evidence for the freeze-concentration factors predicted by the freezing-point depression model. For example, NMR measurements show that the freezing-point depression model reasonably describes the bulk composition of LLRs in ice samples made from NaCl solutions (≥ 1 mM) or seawater.[9] Perhaps because of evidence such as this, the freezing-point depression model is widely used in numerical models of ice and snow (photo)chemistry to describe solute concentrations in the LLRs of ice.[12-17]

Understanding the composition of LLRs is essential, in part, because values of the freeze-concentration factor can significantly influence the (photo)chemistry of trace species on ice and snow.[2,18] For some reactions the chemical behavior in LLRs is similar to liquid-phase chemistry. For example, liquid-phase kinetics and mechanisms can explain the direct photolysis of nitrate, nitrite, and hydrogen peroxide on/in ice made from slowly frozen solutions, conditions where we expect solutes to be in LLRs.[19-23]

However, in many cases liquid-phase chemistry cannot be extrapolated to ice conditions. There are a number of potential causes for chemistry to be enhanced in/on ice, including freezing potential, changes in pH, catalysis or other reactivity enhancement on ice, and/or viscosity changes.[24-27] In addition, the freeze-concentration of solutes into LLRs can significantly alter chemistry in/on ice. Takenaka and coworkers showed that as solutions are frozen, solutes partition out of the ice and form a concentrated brine in the unfrozen portion of the solution, where rates of nitrite oxidation are 10^5 (or more) times faster than in solution.[24,28-31] In frozen solutions, Grannas and coworkers showed enhanced photoreaction rates of *p*-nitroanisole with pyridine and observed rates up to about 40 times

higher on ice than in the corresponding liquid.[32] We have shown that concentrations of singlet molecular oxygen ($^1O_2^*$) on illuminated ice can be 10^4 (or more) times larger than in identical (but unfrozen) illuminated liquid solutions.[33]

While the freeze-concentration of solutes in/on ice and its impacts on chemical reactions have been demonstrated, we do not understand the conditions where liquid-like regions may be described by freezing-point depression model. While the work of Cho and coworkers shows good agreement between experimental results and freezing-point depression,[9] solute concentrations in the pre-frozen solutions were higher than concentrations found in many natural snows. Comparisons between freezing-point depression and lower total solute regimes have not yet been explored. Furthermore, freezing-point depression is traditionally applied to ice samples above their eutectic temperature, where solutes are not expected to completely precipitate. In this work we use the kinetics of singlet molecular oxygen ($^1O_2^*$) to probe the physical nature of LLRs in/on ice and see how their compositions vary with total solute concentration, the identity of the solute, and temperature. In addition, we compare the freeze-concentration factors measured in our ice experiments with those predicted by the freezing-point depression model over a range of conditions.

2. Experimental Methods

2.1 Materials. Furfuryl alcohol (FFA, 98%), Rose Bengal sodium salt (RB, ≥85%), sodium sulfate (Na_2SO_4, SigmaUltra), calcium chloride ($CaCl_2$, 99.99%), and 2-nitrobenzaldehyde (2NB, 98%) were from Sigma-Aldrich. Sodium chloride (NaCl, A.C.S.) and acetonitrile (CH_3CN, HPLC Grade) were from Fisher, while deuterium oxide (D_2O,

>99.95%) was from Acros Organics. Purified water (Milli-Q) was obtained from a Milli-Q Plus system (≥18.2 MΩ cm) with an upstream Barnstead B-Pure carbon cartridge.

2.2 Sample preparation. The majority of samples were prepared in air-saturated Milli-Q water, while a few control experiments were prepared in air-saturated D_2O. The total solute (TS) concentrations of solutions (Equation 1) ranged from 0.020 to 1400 mmol/kg and were controlled using Na_2SO_4, NaCl, or $CaCl_2$; total solute concentrations assume complete dissociation of the salt. To form $^1O_2^*$ in solutions we used RB as the photosensitizer,[34] which has a peak absorption band at 549 nm (Supporting Information, Figure S1). In ice experiments we used ice pellets made from solutions containing 10 nM RB, while for liquid tests (where reaction rates were slower) we used 100 nM RB.

To measure $^1O_2^*$ we used FFA as a chemical probe.[34] In ice experiments the concentration of FFA (10, 30, or 50 nM) was low enough that FFA should have been a minor sink for $^1O_2^*$ in LLRs (i.e., FFA consumed less than 30% of the singlet oxygen), based on calculations using a freezing-point depression (FPD) model (see Supporting Information, Section S1). In liquid samples, we used 50 nM FFA; under these conditions FFA should scavenge < 0.02% of $^1O_2^*$ in either H_2O or D_2O. Our calculations that FFA is a minor sink for $^1O_2^*$ in our experiments are confirmed by experimental results, which show that using 10 or 50 nM of FFA has no effect on the measured rate constant for FFA loss in either liquid or ice (Supporting Information, Figures S2A and S2C).

Solutions for liquid tests were transferred to a 2-cm FUV quartz cuvette (Spectrocell) and cooled to 5˚C before illumination. For ice tests, 720 µL aliquots of solution were pipetted into custom-made PTFE ice pellet molds and slowly frozen at –10˚C in a bench top freeze-chamber. Once solid (after approximately 1 h), samples were transferred

to the illumination system and allowed to equilibrate to the chamber temperature (–5 to –35˚C) for at least 10 minutes before light exposure.

2.3 Illumination and analysis. Samples were illuminated in a temperature-controlled chamber with 549 nm light from a monochromatic illumination system (MIS; Spectral energy) with a 1000-W Hg/Xe lamp.[21] In order to slow down the rate of FFA reaction in ice samples, we added 6 metal screens in the light path to decrease the photon flux; for liquid solutions, where reactions were slower, no metal screens were added. After illumination, samples were allowed to melt in the dark at room temperature and then the entire sample was immediately analyzed for FFA. Samples containing chloride salts were diluted prior to injection with 100 µL of 40 mM Na_2SO_4 to improve peak separation. Illuminated samples were analyzed for FFA concentration using a high-performance liquid chromatograph (HPLC) consisting of: a Shimadzu SPD-10A UV-Vis detector (detection λ = 220 nm), Shimadzu LC-10AT pump, mobile phase of 15% CH_3CN / 85% Milli-Q, flow rate of 0.6 mL min^{-1}, BetaBasic-18 analytical column (250 x 3 mm, 5 µm bead, Thermo Hypersil-Keytone) and guard column, and 400 µL injection loop.

Pseudo first-order rate constants for loss of FFA (k'_{FFA}) were determined from the slope of plots of $\ln([FFA]/[FFA]_0)$ versus illumination time, where [FFA] and $[FFA]_0$ are the concentrations of FFA at some illumination time and time zero, respectively.

2.4. Photon flux measurements and adjustments. The relative photon flux on the day of each experiment was measured using 2NB actinometry to determine j_{2NB}, the rate constant for 2NB loss.[35] Daily actinometry experiments were performed using a liquid solution and/or ice pellets containing 10 µM 2NB and under the same experimental conditions (temperature, cooling/freezing method, sample container) as the corresponding

$^1O_2^*$ experiments, with two exceptions. The first exception is that 2NB was illuminated with 313 nm light (instead of 549 nm light) in order to keep actinometry measurements relatively short. This approach is valid since on a given day the rate constant for 2NB loss with 313 nm light is proportional to (and 260 times faster than) the rate constant with 549 nm light (Supporting Information, Figure S3). Thus, although we cannot use the 313 nm result to determine the absolute photon flux at 549 nm, we can use it to scale our FFA kinetic results to relative changes in the photon flux at 549 nm.

The second exception is that, while $^1O_2^*$ solutions contained various amounts of salts to control the total solute concentration, we measured the daily 2NB actinometry in samples containing no added salts. To be able to adjust each day's ice actinometry to different salt conditions we measured j_{2NB} as a function of total solute concentration for each of the three salts we used in our $^1O_2^*$ experiments. As discussed in section 3.1, we use these results with the daily j_{2NB} rate constant to determine the relative photon flux in each ice sample.

We found that actinometry performed on D_2O-ice at –10˚C is not statistically different than on water-ice at –10˚C. However, 2NB loss on D_2O-ice at –30˚C was about 30% faster than on H_2O- or D_2O-ice at –10 or –30 ˚C (Supporting Information, Figure S2B). We account for this effect in FFA experiments in/on D_2O-ice at –30˚C.

2.5 Calculation of [$^1O_2^*$] and the experimentally determined freeze-concentration factor, F_{Exp}. The measured pseudo-first-order rate constant for FFA loss (k'_{FFA}) is the sum of all FFA loss pathways in an experiment. In our experiments with added Rose Bengal the only significant loss pathways should be $^1O_2^*$ and direct photodegradation and thus

$$k'_{FFA} = k_{FFA+1O2^*}[^1O_2^*] + j_{FFA} \quad (2)$$

where $k_{FFA+1O2^*}$ is the second-order rate constant for reaction of FFA with $^1O_2^*$ (Supporting Information, Section S1), $[^1O_2^*]$ is the steady-state concentration of $^1O_2^*$, and j_{FFA} is the rate constant for direct photodegradation of FFA. Our assumption that other loss pathways for FFA are negligible is validated by results in D_2O, which are discussed in section 3.2. In order to compare ice and liquid results, liquid values of k'_{FFA} were scaled to the concentration of RB on ice (i.e., $k'_{FFA,LIQ}$ was divided by a factor of 10); as shown in Figure S1B of the Supporting Information, values of $k'_{FFA,LIQ}$ are proportional to the Rose Bengal concentration.

For a given experiment, we corrected the measured rate constant for FFA loss to: (1) correct for daily variations in photon flux from our illumination system, (2) account for the effect of salt on effective photon fluxes in the sample, and (3) normalize the result to the modeled photon flux in midday, summer surface snow at Summit, Greenland ($j_{2NB,Sum}$ = 0.022 s^{-1}).[36]

$$k'_{FFA,Sum} = k'_{FFA} \frac{j_{2NB,Sum}}{j_{2NB,Exp}} \frac{j_{2NB}}{j_{2NB,Salt}} \quad (3)$$

In equation 3, $k'_{FFA,Sum}$ is the corrected and normalized pseudo-first order rate constant for loss of FFA and $j_{2NB,Exp}$ is the rate constant for 2NB loss on a given experimental day, measured in a sample with no added salt. The final term ($j_{2NB}/j_{2NB,Salt}$) adjusts for the effects of salt on the effective photon flux in ice samples (see section 3.1); this ratio is 1.0 for liquid solutions.

The value of $k'_{FFA,Sum}$ includes the contributions from both loss pathways for FFA (Equation 2). To calculate experimental values of steady-state $^1O_2^*$ concentrations under

Summit snow conditions, we subtract the direct photodegradation rate constant ($j_{FFA,Sum}$; corrected and normalized for photon flux as in Equation 3) and then divide by the temperature-corrected, second-order rate constant $k_{FFA+1O2*}$ (Supporting Information, Section S1):

$$[^1O_2^*] = \frac{k'_{FFA,Sum} - j_{FFA,Sum}}{k_{FFA+1O2*}} \quad (4)$$

In all liquid experiments, and for ice tests at nearly every total solute concentration, the contribution of $j_{FFA,Sum}$ to $k'_{FFA,Sum}$ was negligible. The few exceptions, along with results of control experiments for direct photodegradation of FFA, are detailed in the Supplemental Information (Section S2).

For liquid samples (100 nM RB, 5˚C), the concentration of $^1O_2^*$ decreased by about 40% as total solute concentrations were increased from 0.02 to 1400 mmol/kg (Supporting Information, Figure S4). We account for this small decrease by calculating our liquid $^1O_2^*$ concentrations from the empirical relationship derived from Figure S4:

$$[^1O_2^*]_{LIQ} = -0.025 \pm 0.0057 \ln[TS] + 0.60 \pm 0.021 \quad (5)$$

where $[^1O_2^*]_{LIQ}$ is the liquid steady-state concentration of $^1O_2^*$ (normalized to summer Summit snow sunlight conditions; units of picomolar) and [TS] is in units of mmol/kg. For the same solution studied as both ice and liquid, we use measured Summit-sunlight-normalized steady-state $^1O_2^*$ concentrations on ice ($[^1O_2^*]_{LLR}$) and in liquid to experimentally determine the freeze-concentration factor (F_{Exp}):

$$F_{Exp} = \frac{[^1O_2^*]_{LLR}}{[^1O_2^*]_{LIQ}} \quad (6)$$

Unless otherwise noted, uncertainties listed for all values, and error bars on all figures, are the calculated standard errors (±1 SE) propagated from the measured relative standard error of each component.

3. Results and Discussion

3.1 Effect of salt on photon fluxes in/on ice. Because the photon flux is one of the essential quantities that determine the rate of a photochemical reaction, we first examined how the 2NB actinometry of ice depends on the identity and concentration of salt. As shown in Figure 1, in all cases the loss of 2NB is faster in ice pellets made from solutions containing salt; i.e., the presence of salt increases the effective photon flux in LLRs.

For ice pellets made from sodium sulfate solutions, photolysis of 2NB is enhanced (compared to pellets with no added Na_2SO_4) but independent of salt concentration, with an average value of $j_{2NB,Salt}/j_{2NB}$ of 1.62 ± 0.094 s^{-1}/s^{-1} (Figure 1A). Samples containing NaCl or $CaCl_2$ behaved very similarly to each other, but with two regimes for 2NB loss: (1) a linear increase in $j_{2NB,Salt}$ with total solute concentration up to 7.8 mmol/kg ($j_{2NB,Salt}/j_{2NB}$ (units of s^{-1}/s^{-1}) = (0.14 ± 0.019)[TS] + (1.12 ± 0.089), R^2 = 0.85; Figure 1B, Inset) and (2) a constant value ($j_{2NB,Salt}/j_{2NB}$ = 2.24 ± 0.095 s^{-1}/s^{-1}) at higher total solute concentrations (7.8 to 1400 mmol/kg; Figure 1B). As is the case throughout the manuscript, total solute concentrations listed here are those of the original liquid solution used to make the ice pellets.

We also measured j_{2NB} in several NaCl ice samples at –30 λC, but these results were not different from those at –10 ° C, indicating that temperature does not affect j_{2NB} or the impact of salts; this is consistent with the lack of temperature dependence seen in ice samples made without salt.[35] The total solute concentration had no effect (for any of the salts) on 2NB actinometry in liquid (i.e., $j_{2NB,Salt}/j_{2NB}$= 1.0).

As far as we are aware, this is the first time the effect of solutes on the effective photon flux in ice samples has been characterized. Although we do not understand the mechanism, the enhanced photochemical loss of 2NB in frozen samples in the presence of salt illustrates the importance of measuring photon fluxes in laboratory ices (and of normalizing rates to measured photon fluxes). These results also suggest that photon fluxes (and thus photochemical rates) in natural ice and snow might sometimes be enhanced by salts.

3.2 D_2O as a diagnostic test for $^1O_2^*$. Singlet molecular oxygen is a reactive intermediate that forms when an organic chromophore absorbs light, transitions to an excited state, and subsequently transfers energy to dissolved (ground state, triplet) O_2.[34,37-40] In ice pellets containing the $^1O_2^*$ sensitizer Rose Bengal, we expect that $^1O_2^*$ is the dominant sink for FFA. To test this expectation, we measured FFA loss in parallel ice pellets made from H_2O or D_2O, a diagnostic test that has been previously used in solution.[41-43] In aqueous solution, H_2O (or D_2O) is the dominant sink for $^1O_2^*$. Thus, since the room temperature deactivation rate constant of $^1O_2^*$ with D_2O (k'_{D2O} = 1.6 ° 10^4 s^{-1}; ref. 43) is 13.8 times slower than in H_2O (k'_{H2O} = 2.2 $\times 10^5$ s^{-1}; ref. 43) the steady-state concentration of $^1O_2^*$ (and, thus, $k'_{FFA,Sum}$) should be 14 times higher in D_2O than in H_2O.

While this diagnostic test has not been previously used with ice samples, it should work at least qualitatively. One complication is that the cryoscopic constant (E_f) for D_2O is not the same as for H_2O: as described in the Supporting Information (Section S3), E_f for D_2O is 1.1 times greater than for H_2O. This difference in E_f has the effect of reducing F_{FPD} for a given set of T and total solute conditions, thereby reducing $^1O_2^*$ concentrations on D_2O-ice compared to the equivalent conditions in/on H_2O-ice. A second complication is that the

freezing temperature for D_2O ($T_{f,D2O}$ = 3.7˚C)[44] is higher than for H_2O, which increases F_{FPD}, although this factor is less pronounced at lower temperatures. With these combined effects the concentration of $^1O_2$* (and value of $k'_{FFA,Sum}$) in ice LLRs at –10˚C should be 16.6 times higher with D_2O-ice compared to H_2O-ice; at –30˚C this factor is 13.9.

Our experimental results in D_2O are generally consistent with these calculated factors, but not to the full extent expected. At –10˚C, for ice made from solutions containing identical solutes (10 nM RB, 50 nM FFA, and 6 mmol/kg TS as NaCl), $k'_{FFA,Sum}$ is 9.3 ± 5.0 times faster on D_2O-ice than on H_2O-ice (Supporting Information, Figure S2C). At –30˚C, which is below the eutectic temperature of NaCl, FFA loss is 7.0 ± 3.5 times faster with D_2O-ice than with ice made from H_2O (Figure S2C). While these D_2O enhancements are 1.8 and 2.0 times lower than expected (at –10 and –30 ˚C, respectively), they are qualitatively consistent with what is expected if $^1O_2$* is the dominant oxidant in our RB-containing samples. The difference between the calculated and measured D_2O enhancements might be due to dilution of D_2O in LLRs at the air-ice interface by condensation of H_2O vapor from the atmosphere. On this note, a decrease of the D_2O mole fraction from 100 to 92% in LLRs would account for the missing factor of 2 in the expected enhancement of $^1O_2$* and $k'_{FFA,Sum}$ on D_2O.

3.3 Effect of solute identity and concentration on furfuryl alcohol loss in/on ice. The freezing-point depression model (Equation 1) indicates that the volume of LLRs will be lower in/on ices made from solutions with lower initial total solute concentrations. Thus in ice made from lower total solute solutions, the LLR concentrations of $^1O_2$* precursors (e.g., RB in our experiments) will increase while the $^1O_2$* sink (i.e., water) will be approximately constant: the net effect is higher concentrations of $^1O_2$* and faster losses of

FFA with decreasing total solute concentrations.[33] Figure 2 shows kinetic data for FFA loss on ice made from solutions with different solutes and solute concentrations. While these are raw data (i.e., they do not contain the corrections for photon flux or for the minor effect of direct photodegradation of FFA), they show the general effect of solutes on FFA kinetics and $^1O_2^*$ steady-state concentrations in LLRs: For all salt types, the rate constant for FFA loss decreases with increasing total solute concentration. However, the effect of increasing total solutes on the rate constant of FFA loss is muted for Na_2SO_4 when compared to the chloride salts, which show considerably slower loss at the highest total solute concentrations. For example, the lifetimes of FFA ($\tau_{FFA} = k'^{-1}_{FFA}$) at the highest total solute concentrations were 3, 66, and 390 times larger than at the lowest total solute concentrations for Na_2SO_4, NaCl, and $CaCl_2$, respectively.

The effect of total solute levels in these data is also apparent when comparing steady-state $^1O_2^*$ concentrations at the extremes of total solute concentration. To estimate $^1O_2^*$ concentrations from the raw data, we use a simplified form of Equation 2, namely $[^1O_2^*] = k'_{FFA}/k_{FFA+1O2^*}$. As shown in Figure 2, at the lowest concentrations of total solutes, the concentration of $^1O_2^*$ is similar for all three salts (0.3 – 0.7 nM), while values at the highest total solute concentrations vary widely between salts, with Na_2SO_4 showing the least sensitivity to changes in solute levels.

The solute concentration dependence of the $^1O_2^*$ concentrations in Figure 2 qualitatively show the behavior expected from the freeze-concentration of solutes: decreasing the solute concentration of the liquid solution leads to an increase in the freeze-concentration factor (F_{FPD}) for the corresponding ice samples, thereby increasing the concentration of $^1O_2^*$ in liquid-like regions of the ice (Equation 1).

3.4 Effects of total solute concentrations on freeze-concentration factors. While the raw data in Figure 2 qualitatively show the expected behavior of total solute concentrations on chemistry in LLRs, we can more quantitatively examine this relationship. To do this, we account for differences in photon fluxes (Equation 3), subtract the minor contribution of direct photodegradation of FFA (Equation 4), and convert our rate constants for FFA loss to steady-state concentrations of $^1O_2^*$ (Equation 4). We then use the ratio of $[^1O_2^*]$ in liquid and ice samples of the same composition to experimentally determine the freeze-concentration factor (F_{Exp}, Equation 5). Figure 3 shows the effect of different salts and total solute concentrations on F_{Exp}, along with calculated values of F_{FPD} from the freezing-point depression model. While F_{Exp} decreases with increasing total solutes for all three salts, the results for each salt sometimes show large differences.

In the case of Na_2SO_4 as the total solute control, for ice at –10˚C F_{Exp} changes very little over the range of total solute concentrations (Figure 3A), with an average (± 1 SE) value of $(4.8 \pm 0.73) \times 10^3$. While not statistically significant at a 95% confidence interval, there is a slight increase from $(2.1 \pm 0.89) \times 10^3$ to $(5.3 \pm 2.2) \times 10^3$ as the total solute concentration in the solution decreases from 1400 to 0.03 mmol/kg; i.e., F_{Exp} increases by only a factor of 2.5 as total solutes decrease by a factor of 45000. At total solute concentrations less than about 1 mmol/kg, F_{FPD} over-estimates F_{Exp}; this difference increases with decreasing solute. Above ~1 mmol/kg TS the reverse is true: F_{FPD} under-estimates F_{Exp} and this difference becomes larger with increasing solute concentration.

The likely explanation for this discrepancy between F_{FPD} and F_{Exp} is that the experimental temperature (–10 ˚C) is below the eutectic temperature (T_{eu}) of Na_2SO_4-H_2O (–1.3˚C),[45,46] i.e., the temperature below which a system should form a solid mixture of pure

ice and precipitated salt.[45,47] Although all of the salt should be precipitated below the eutectic temperature based on the common definition of T_{eu}, there is evidence that liquid-brine layers do exist.[9,32,48] So the fact that the Na_2SO_4 ice samples in Figure 3 were studied at a temperature below T_{eu} does not preclude some effect of freeze-concentration, but likely explains the insensitivity of F_{Exp} to total solutes for Na_2SO_4-ice.

In contrast to the Na_2SO_4 results, frozen chloride-salt solutions at −10˚C (above their eutectic temperatures) show much more variation in F_{Exp} with changes in total solute concentration (Figures 3B and 3C). For ices containing NaCl (T_{eu} = −21.5˚C)[46], values of F_{Exp} increase from 8.0 ± 3.5 to (1.6 ± 0.85) $\times 10^4$, a factor of ~2000 increase, as the total solute concentration in the precursor solution decreases from 1230 to 0.02 mmol/kg. We verified that Cl^- does not appreciably scavenge the RB triplet by measuring FFA loss in ice with 0.065 mmol/kg $NaNO_3$ as the total solute control; this result was comparable to the NaCl and $CaCl_2$ results. Figure 3B also shows that our values of F_{Exp} at −10˚C are very similar to those measured by Cho and coworkers using proton NMR.[9] For $CaCl_2$ (T_{eu} = −49.5˚C)[46] our values of F_{Exp} increase from 0.87 ± 0.41 to (9.8 ± 4.3) $\times 10^3$, a factor of ~11000 increase, over a decrease in total solute concentration from 1400 to 0.02 mmol/kg.

There appear to be two general F_{Exp} regimes for the chloride salts. First, at total solute concentrations less than approximately 1 mmol/kg, the chloride salt ices have values for F_{Exp} that are roughly 2 to 20 times lower than calculated by freezing-point depression, similar to what we observe in Na_2SO_4 samples. In the second regime, near 1 mmol/kg TS and above, F_{Exp} appears to converge to F_{FPD} for ice containing NaCl, while F_{Exp} for ice containing $CaCl_2$ appears to be bounded by F_{FPD} (Figures 3B and 3C). In the case of $CaCl_2$, the experimental underestimate of F_{FPD} at high $CaCl_2$ concentrations could be due to the fact

that the majority of FFA loss is due to direct photodegradation in this TS regime (i.e., in this case, the estimate of F_{Exp} requires parsing the minor contribution of $^1O_2$* from the major contribution of direct photodegradation to loss of FFA). Although we correct for direct photodegradation, the large size of $j_{FFA,Sum}$ makes our calculation of [$^1O_2$*], and thus F_{Exp}, more uncertain.

We also tested the effect of total solute concentration on NaCl ice samples illuminated below the eutectic temperature, at –30˚C (Figure 3B). As shown by the gray line in Figure 3B, the freezing-point depression model predicts that freeze-concentration factors at –30˚C are simply enhanced by a factor of 3 compared to the –10˚C values. In our experiments, measured values of F_{Exp} are higher at –30˚C compared to at –10˚C, but with enhancement factors that range from 11 at the highest total solute concentration to 1.5 at the lowest. At total solute concentrations of 6 mmol/kg and below, F_{Exp} values at –30˚C are similar to values at –10˚C and are also lower than predicted from the freezing-point depression model. However, at 60 mmol/kg TS and above, F_{Exp} for NaCl ice at –30˚C is 3 to 7 times higher than F_{FPD}. While this general behavior is similar to the subeutectic case with Na_2SO_4, the effect is far less pronounced with NaCl. For NaCl at –30˚C, F_{Exp} ranges from 86 ± 38 to $(2.1 \pm 0.98) \times 10^4$ from 1230 to 0.02 mmol/kg TS, an increase by a factor of ~240 over the total solute range; in contrast, F_{Exp} for Na_2SO_4 at –10˚C is essentially constant over a similar concentration range. Although F_{Exp} is less sensitive to changes in total solutes for NaCl-ice below the eutectic temperature, this ice still exhibits behavior consistent with LLRs whose compositions vary qualitatively as expected from a freezing-point depression model.

To more quantitatively describe the conditions under which liquid-like regions may be best modeled with freezing-point depression, in Figure 4 we compare the ratio of F_{Exp} to F_{FPD} over the range of total solute concentrations. At the lowest total solute concentrations, measured values of the freeze-concentration factor are approximately 30–60 times lower than predicted from freezing-point depression, both for ices studied above and below their eutectic temperature (Figures 4A and 4B). This difference between F_{Exp} and F_{FPD} decreases with increasing total solutes, disappearing at approximately 1–3 mmol/kg TS. At total solute levels above this concentration, whether the system is above or below T_{eu} becomes more important. For systems below T_{eu}, F_{Exp} exceeds F_{FPD} for total solute concentrations above 6 mmol/kg, with the ratio F_{Exp}:F_{FPD} reaching 6.4 at 1230 mmol/kg TS for NaCl (at –30˚C) and 520 at 1400 mmol/kg Na_2SO_4. For systems above T_{eu} and with total solute concentrations above approximately 1 mmol/kg, F_{Exp} is fairly well described by F_{FPD} for NaCl-ice, while for the highest concentrations of $CaCl_2$-ice the measured value of F is 11 to 14 times lower than predicted by the freezing-point depression model. Ratios calculated from NaCl data of Cho and coworkers[9] in this solute range are similarly well described by freezing-point depression (Figure 4A). Regardless of whether the temperature of the system is above or below T_{eu}, freezing-point depression predicts F_{Exp} within a factor of 5 for the small total solute concentration range between 0.5 and 1.8 mmol/kg. If we exclude Na_2SO_4-ice from this comparison, the solute range expands to 0.5 to 18.5 mmol/kg (Figure 4).

3.5 Effect of temperature on the freeze-concentration factor. In addition to the impact of total solute levels described above, changes in temperature also affect the composition of LLRs and the freeze-concentration factor F_{FPD} (Equation 1). To examine this

effect we selected a total solute concentration where F_{Exp} and F_{FPD} are similar in our NaCl experiments (6 mmol/kg TS) and made measurements of $^1O_2$* as a function of temperature. As shown in Figure 5A, values of F_{Exp} increase by a factor of approximately 6, from 710 ± 390 to 4300 ± 2000, as the temperature decreases from –5 to –35 ˚C. Over this temperature range freezing-point depression describes F_{Exp} very well both above and below the eutectic temperature, within a factor of 1.6 over the entire temperature range (Figure 5B). This good agreement between F_{Exp} and F_{FPD} suggests that NaCl remains in LLRs that follow freezing-point depression behavior to temperatures at least as low as –35 ˚C. As illustrated by the crosses in Figure 5, Cho and coworkers found a similar result: if the total solute concentration in the pre-frozen solution was below approximately 20 mmol/kg more than half of the initial Na^+ remained in liquid-like regions to temperatures as low as –43 ˚C.[9] Grannas and coworkers found this minimum concentration of NaCl could be as high as 155 mmol/kg with little precipitation of the salt in ice.[32] Thus while freezing-point depression does a poor job of describing the freeze-concentration factor at low total solute concentrations (Figure 3), with 6 mmol/kg TS as NaCl (and presumably other concentrations near 0.5–18.5 mmol/kg TS), the freezing-point depression model accurately matches our experimental results down to temperatures at least 14˚C lower than the eutectic temperature for the system (Figure 5).

3.6 Possible reasons for the disagreement between measured and modeled freeze-concentration factors. At solute concentrations below 1 mmol/kg our measured values of F_{Exp} are less sensitive to total solute concentrations than predicted from freezing-point depression, with all three salts giving nearly the same concentration factor (F_{Exp} ~ 10^4) at very low total solute levels. Why are our measured values of F lower than those

predicted from freezing-point depression under low total solute conditions? Grannas and coworkers observed a similar behavior for the photoreactivity of *p*-nitroanisole on ice: reactivity increased as the total solute (NaCl) concentration decreased until around 7.5 mmol/kg (at –10˚C) when the reactivity leveled off, which they attributed to solute precipitation.[32] However, we think it is unlikely that FFA is precipitating at the highest values of *F* in our experiments (i.e., under conditions of lowest total solutes) where the concentration of solutes should be enhanced by factors greater than 10,000. At room-temperature FFA is miscible in water.[34,49] In the case of FFA, even with our greatest measured value of *F* the concentration of FFA in liquid-like regions would be only approximately 2.7 mM; thus precipitation should not occur. In the case of RB, which has a solubility of ~1 mM at room temperature,[50] we start with 10 nM in our pre-frozen solutions so that RB precipitation should not occur for freeze-concentration factors as large as 10^5. A concentration factor of 10^5 corresponds to an initial total solute concentration of 0.054 mmol/kg at -10˚C, well below the range of 1 mmol/kg where F_{Exp} begins to deviate from F_{FPD}. It is possible, however, that at the low temperatures of our ice experiments that the solubility of RB is decreased, resulting in RB precipitation. Another possibility is that RB is aggregating in highly concentrated LLRs, which could reduce $^1O_2$* formation by decreasing RB light absorption.[50,51] Finally, non-ideal behavior in our samples cannot explain the discrepancy between F_{FPD} and F_{Exp} in the low TS regime: adjusting for non-ideality across our total solute range by applying results of Kuo and coworkers[16] yields little difference in F_{FPD}, with the largest difference only a factor of ~1.3 lower at the lowest TS concentrations. Thus we cannot currently explain why our results do not match freezing-point depression predictions at low TS conditions.

4. Conclusions

Snow and ice provide a vast surface area for chemical reactions that can affect the chemistry of the overlying atmosphere as well as the water that drains into soils and surface waters after snowmelt. In the environment, the total concentration of solutes in snow and ice can vary widely, from 10's of micromolar in clean continental snows[52-54] to molar levels in sea-ice brines and frost flowers.[55] This total solute concentration, along with temperature, controls the volume of liquid-like regions in/on snow and ice.

We have shown that measured concentration enhancements in LLRs are well described by freezing-point depression under some conditions. For example, in systems containing chloride salts, freezing-point depression describes F_{Exp} when total solute concentrations are above ~1 mmol/kg at a range of temperatures above and – somewhat surprisingly – below the eutectic temperature. Below 1 mmol/kg of total solutes, however, F_{Exp} in NaCl ices is less sensitive to total solute concentration than predicted from freezing-point depression. At low total solute concentrations, we measure freeze-concentration factors as high as 25,000; as far as we can determine, these are the highest experimentally measured values of F, although they are below predicted values. Interestingly, under these low total solute conditions all three of the salts exhibited similar values of F_{Exp}, even though the Na_2SO_4 ice was below its eutectic temperature. Finally, the ~10^4-fold enhancements in $^1O_2$* concentration in LLRs at environmentally relevant low total solute concentrations suggests that singlet oxygen is likely significant in the oxidation of trace species in ice/snow, which is a topic we are currently investigating.

Acknowledgements

This research has been supported by a graduate fellowship (grant # FP916999) to J.B. from the U.S. Environmental Protection Agency's Science to Achieve Results (STAR) program. Although the research described in the article has been funded in part by the U.S. EPA, it has not been subject to any EPA review and therefore does not necessarily reflect the views of the Agency, and no official endorsement should be inferred. We are also grateful for funding from the National Science Foundation (grant # CHE-1214121). Special thanks to Andrew Jilwan and Dana Norall for assistance with experiments and Harry Beine and Bill Casey for comments that improved the manuscript.

Supporting Information Available: Supporting information contains figures that show the dependence of $^1O_2^*$ on RB concentration in solution (Figure S1), control experiments (Figure S2), 2-nitrobenzaldehyde data at 313 and 549 nm (Figure S3), variations of $^1O_2^*$ with total solute concentration in solution (Figure S4), and the dependence of $^1O_2^*$ on RB concentration in/on ice (Figure S5). We also provide information on the temperature correction of rate constants (Section S1), controls for direct photodegradation of FFA (Section S2), and thermodynamic information for D_2O (Section S3). This material is available free of charge via the Internet at http://pubs.acs.org.

References

(1) Rosenberg, R. Why Is Ice Slippery? *Phys. Today* **2005**, *58*, 50-55.
(2) Dominé, F.; Albert, M.; Huthwelker, T.; Jacobi, H. W.; Kokhanovsky, A. A.; Lehning, M.; Picard, G.; Simpson, W. R. Snow Physics as Relevant to Snow Photochemistry. *Atmos. Chem. Phys.* **2008**, *8*, 171-208.
(3) Sadtchenko, V.; Brindza, M.; Chonde, M.; Palmore, B.; Eom, R. The Vaporization Rate of Ice at Temperatures near Its Melting Point. *J. Chem. Phys.* **2004**, *121*, 11980-11992.

(4) Sadtchenko, V.; Ewing, G. E. Interfacial Melting of Thin Ice Films: An Infrared Study. *J. Chem. Phys.* **2002**, *116*, 4686-4697.
(5) Doppenschmidt, A.; Butt, H. J. Measuring the Thickness of the Liquid-Like Layer on Ice Surfaces with Atomic Force Microscopy. *Langmuir* **2000**, *16*, 6709-6714.
(6) Wei, X.; Miranda, P. B.; Shen, Y. R. Surface Vibrational Spectroscopic Study of Surface Melting of Ice. *Phys. Rev. Lett.* **2001**, *86*, 1554-1557.
(7) Kahan, T. F.; Reid, J. P.; Donaldson, D. J. Spectroscopic Probes of the Quasi-Liquid Layer on Ice. *J. Phys. Chem. A* **2007**, *111*, 11006-11012.
(8) Wettlaufer, J. S. Impurity Effects in the Premelting of Ice. *Phys. Rev. Lett.* **1999**, *82*, 2516-2519.
(9) Cho, H.; Shepson, P. B.; Barrie, L. A.; Cowin, J. P.; Zaveri, R. A. Nmr Investigation of the Quasi-Brine Layer in Ice/Brine Mixtures. *J. Phys. Chem. B* **2002**, *106*, 11226-11232.
(10) Haynes, W. M., Ed. Cryoscopic Constants for Calculation of Freezing Point Depression. In *Handbook of Chemistry and Physics, 92nd Edition, Internet Version*; CRC Press/Taylor and Francis: Boca Raton, FL, 2012.
(11) Robinson, C.; Boxe, C. S.; Guzman, M. I.; Colussi, A. J.; Hoffmann, M. R. Acidity of Frozen Electrolyte Solutions. *J. Phys. Chem. B* **2006**, *110*, 7613-7616.
(12) Thomas, J. L.; Stutz, J.; Lefer, B.; Huey, L. G.; Toyota, K.; Dibb, J. E.; von Glasow, R. Modeling Chemistry in and above Snow at Summit, Greenland - Part 1: Model Description and Results. *Atmos. Chem. Phys.* **2011**, *11*, 4899-4914.
(13) Boxe, C. S.; Saiz-Lopez, A. Influence of Thin Liquid Films on Polar Ice Chemistry: Implications for Earth and Planetary Science. *Polar Sci.* **2009**, *3*, 73-81.
(14) Boxe, C. S.; Saiz-Lopez, A. Multiphase Modeling of Nitrate Photochemistry in the Quasi-Liquid Layer (Qll): Implications for No(X) Release from the Arctic and Coastal Antarctic Snowpack. *Atmos. Chem. Phys.* **2008**, *8*, 4855-4864.
(15) Jacobi, H.-W.; Hilker, B. A Mechanism for the Photochemical Transformation of Nitrate in Snow. *J. Photochem. Photobio. A* **2007**, *185*, 371-382.
(16) Kuo, M. H.; Moussa, S. G.; McNeill, V. F. Modeling Interfacial Liquid Layers on Environmental Ices. *Atmos. Chem. Phys.* **2011**, *11*, 9971-9982.
(17) Liao, W.; Tan, D. 1-D Air-Snowpack Modeling of Atmospheric Nitrous Acid at South Pole During Antci 2003. *Atmos. Chem. Phys.* **2008**, *8*, 7087-7099.
(18) Grannas, A. M.; Jones, A. E.; Dibb, J.; Ammann, M.; Anastasio, C.; Beine, H. J.; Bergin, M.; Bottenheim, J.; Boxe, C. S.; Carver, G.et. al.,. An Overview of Snow Photochemistry: Evidence, Mechanisms and Impacts. *Atmos. Chem. Phys.* **2007**, *7*, 4329-4373.
(19) Boxe, C. S.; Colussi, A. J.; Hoffmann, M. R.; Perez, I. M.; Murphy, J. G.; Cohen, R. C. Kinetics of No and No2 Evolution from Illuminated Frozen Nitrate Solutions. *J. of Phys. Chem. A* **2006**, *110*, 3578-3583.
(20) Chu, L.; Anastasio, C. Quantum Yields of Hydroxyl Radical and Nitrogen Dioxide from the Photolysis of Nitrate on Ice. *J. Phys. Chem. A* **2003**, *107*, 9594-9602.
(21) Chu, L.; Anastasio, C. Formation of Hydroxyl Radical from the Photolysis of Frozen Hydrogen Peroxide. *J. Phys. Chem. A* **2005**, *109*, 6264-6271.
(22) Dubowski, Y.; Colussi, A. J.; Hoffmann, M. R. Nitrogen Dioxide Release in the 302 Nm Band Photolysis of Spray-Frozen Aqueous Nitrate Solutions. Atmospheric Implications. *J. Phys. Chem. A* **2001**, *105*, 4928-4932.

(23) Honrath, R. E.; Guo, S.; Peterson, M. C.; Dziobak, M. P.; Dibb, J. E.; Arsenault, M. A. Photochemical Production of Gas Phase No_x from Ice Crystal No_3^-. *J. Geo. Res.* **2000**, *105*, 24183-24190.
(24) Takenaka, N.; Bandow, H. Chemical Kinetics of Reactions in the Unfrozen Solution of Ice. *J. Phys. Chem. A* **2007**, *111*, 8780–8786.
(25) Fennema, O. Activity of Enzymes in Partially Frozen Aqueous Systems. In *Water Relations of Foods*; Duckworth, R. B., Ed.; Academic Press: London, **1975**.
(26) Fennema, O. Reaction Kinetics in Partially Frozen Aqueous Systems. In *Water Relations of Foods*; Duckworth, R. B., Ed.; Academic Press: London, **1975**.
(27) Kahan, T. F.; Kwamena, N. O. A.; Donaldson, D. J. Different Photolysis Kinetics at the Surface of Frozen Freshwater Vs. Frozen Salt Solutions. *Atmos. Chem. Phys.* **2010**, *10*, 10917-10922.
(28) Takenaka, N.; Takahashi, I.; Suekane, H.; Yamamoto, K.; Sadanaga, Y.; Bandow, H. Acceleration of Ammonium Nitrite Denitrification by Freezing: Determination of Activation Energy from the Temperature of Maximum Reaction Rate. *J. Phys. Chem. A* **2011**, *115*, 14446-14451.
(29) Takenaka, N.; Ueda, A.; Daimon, T.; Bandow, H.; Dohmaru, T.; Maeda, Y. Acceleration Mechanism of Chemical Reaction by Freezing: The Reaction of Nitrous Acid with Dissolved Oxygen. *J. Phys. Chem. A* **1996**, *100*, 13874-13884.
(30) Takenaka, N.; Ueda, A.; Maeda, Y. Acceleration of the Rate of Nitrite Oxidation by Freezing in Aqueous-Solution. *Nature* **1992**, *358*, 736-738.
(31) Takenaka, N.; Daimon, T.; Ueda, A.; Sato, K.; Kitano, M.; Bandow, H.; Maeda, Y. Fast Oxidation Reaction of Nitrite by Dissolved Oxygen in the Freezing Process in the Tropospheric Aqueous Phase. *J. Atmos. Chem.* **1998**, *29*, 135-150.
(32) Grannas, A. M.; Bausch, A. R.; Mahanna, K. M. Enhanced Aqueous Photochemical Reaction Rates after Freezing. *J. Phys. Chem. A* **2007b**, *111*, 11043-11049.
(33) Bower, J.; Anastasio, C. Measuring the 10,000-Fold Enhancement of Singlet Molecular Oxygen on Illuminated Ice Relative to the Corresponding Liquid Solution. *Atmos. Environ.* **2013**, *75*, 188-195.
(34) Haag, W. R.; Hoigne, J.; Gassman, E.; Braun, A. M. Singlet Oxygen in Surface Waters .1. Furfuryl Alcohol as a Trapping Agent. *Chemosphere* **1984**, *13*, 631-640.
(35) Galbavy, E. S.; Ram, K.; Anastasio, C. 2-Nitrobenzaldehyde as a Chemical Actinometer for Solution and Ice Photochemistry. *J. Photochem. Photobiol. A* **2010**, *209*, 186-192.
(36) Ram, K.; Anastasio, C. Photochemistry of Phenanthrene, Pyrene, and Fluoranthene in Ice and Snow. *Atmos. Environ.* **2009**, *43*, 2252-2259.
(37) Abdel-Shafi, A. A.; Worrall, D. R.; Wilkinson, F. Singlet Oxygen Formation Efficiencies Following Quenching of Excited Singlet and Triplet States of Aromatic Hydrocarbons by Molecular Oxygen. *J. Photochem. Photobiol. A* **2001**, *142*, 133-143.
(38) Haag, W. R.; Hoigne, J. Singlet Oxygen in Surface Waters .3. Photochemical Formation and Steady-State Concentrations in Various Types of Waters. *Environ. Sci. Technol.* **1986**, *20*, 341-348.
(39) Haag, W. R.; Hoigne, J.; Gassman, E.; Braun, A. M. Singlet Oxygen in Surface Waters .2. Quantum Yields of Its Production by Some Natural Humic Materials as a Function of Wavelength. *Chemosphere* **1984**, *13*, 641-650.
(40) Zepp, R. G.; Wolfe, N. L.; Baughman, G. L.; Hollis, R. C. Singlet Oxygen in Natural-Waters. *Nature* **1977**, *267*, 421-423.

(41) Faust, B. C.; Allen, J. M. Aqueous-Phase Photochemical Sources of Peroxyl Radicals and Singlet Molecular-Oxygen in Clouds and Fog. *J. Geo. Res.* **1992**, *97*, 12913-12926.
(42) Anastasio, C.; McGregor, K. G. Chemistry of Fog Waters in California's Central Valley: 1. In Situ Photoformation of Hydroxyl Radical and Singlet Molecular Oxygen. *Atmos. Environ.* **2001**, *35*, 1079-1089.
(43) Bilski, P.; Holt, R. N.; Chignell, C. F. Properties of Singlet Molecular Oxygen $O_2(^1\Delta_G)$ in Binary Solvent Mixtures of Different Polarity and Proticity. *J. Photochem. Photobiol. A* **1997**, *109*, 243-249.
(44) Smirnova, N. N.; Bykova, T. A.; Van Durme, K.; Van Mele, B. Thermodynamic Properties of Deuterium Oxide in the Temperature Range from 6 to 350 K. *J. Chem. Thermodyn.* **2006**, *38*, 879-883.
(45) Hall, C.; Hamilton, A. The Heptahydrate of Sodium Sulfate: Does It Have a Role in Terrestrial and Planetary Geochemistry? *Icarus* **2008**, *198*, 277-279.
(46) Marion, G. M.; Grant, S. A. Frezchem: A Chemical Thermodynamic Model for Electrolyte Solutions at Subzero Temperatures; USACRREL: Hanover, NH, 1994.
(47) Thomsen, K. Aqueous Electrolytes: Model Parameters and Process Simulation. Dissertation, Technical University of Denmark, **1997**.
(48) Koop, T.; Kapilashrami, A.; Molina, L. T.; Molina, M. J. Phase Transitions of Sea-Salt/Water Mixtures at Low Temperatures: Implications for Ozone Chemistry in the Polar Marine Boundary Layer. *J. Geo. Res.* **2000**, *105*, 26393-26402.
(49) Bentley, H. R.; Whitehead, J. K. Water-Miscible Solvents in the Separation of Amino-Acids by Paper Chromatography. *Biochem. J* **1950**, *46*, 341-345.
(50) Neckers, D. C. Rose-Bengal. *J. Photochem. Photobiol. A* **1989**, *47*, 1-29.
(51) Valdes-Aguilera, O.; Neckers, D. C. Properties of Rose-Bengal .27. Rose-Bengal Ethyl-Ester Aggregation in Aqueous-Solution. *J. Phys. Chem.* **1988**, *92*, 4286-4289.
(52) Bower, J. P.; Hood, E.; Hoferkamp, L. A. Major Solutes, Metals, and Alkylated Aromatic Compounds in High-Latitude Maritime Snowpacks near the Trans-Alaska Pipeline Terminal, Valdez, Alaska. *Environ. Res. Lett.* **2008**, *3*, 1-8.
(53) Douglas, T. A.; Sturm, M. Arctic Haze, Mercury and the Chemical Composition of Snow across Northwestern Alaska. *Atmos. Environ.* **2004**, *38*, 805-820.
(54) Whitlow, S.; Mayewski, P. A.; Dibb, J. E. A Comparison of Major Chemical-Species Seasonal Concentration and Accumulation at the South-Pole and Summit, Greenland. *Atmos. Environ.* **1992**, *26*, 2045-2054.
(55) Simpson, W. R.; Alvarez-Aviles, L.; Douglas, T. A.; Sturm, M.; Domine, F. Halogens in the Coastal Snow Pack near Barrow, Alaska: Evidence for Active Bromine Air-Snow Chemistry During Springtime. *Geo. Res. Lett.* **2005**, *32*, 4285-4403.

Figure captions

Figure 1. Effect of total solute concentration, [TS], on 2-nitrobenzaldehyde (2NB) actinometry (i.e., volume-averaged photon flux) on ice at –10 °C. Panel (A) shows that addition of sodium sulfate increases the rate constant for 2NB loss by a factor of 1.6 compared to the case of no added salt. Panel (B) shows results for ice samples made with NaCl (circles) and $CaCl_2$ (triangles): a linear increase in $j_{2NB,Salt}$ between 0 and 7.8 mmol/kg solute and a plateau at higher total solute concentrations. The two values with the highest total solute concentrations (1230 mmol/kg NaCl and 1400 mmol/kg $CaCl_2$) are included in the plateau average but are not shown on the graph (2.3 s^{-1}/s^{-1} and 2.1 s^{-1}/s^{-1} for NaCl and $CaCl_2$, respectively).

Figure 2. Raw data showing the loss of furfuryl alcohol (FFA) in/on ice containing 10 nM Rose Bengal and different total solute (TS) concentrations, adjusted with Na_2SO_4 (A), NaCl (B), or $CaCl_2$ (C). The slope for each regression line is the negative of the first-order rate constant for FFA loss (k'_{FFA}). In each panel the calculated singlet oxygen concentrations are shown for the ice pellets with the highest and lowest total solute concentrations. Results here are raw data and are not corrected for the effect of salt on j_{2NB} or normalized to the reference j_{2NB} value.

Figure 3. Effect of salt type (Na_2SO_4 (A), NaCl (B), and $CaCl_2$ (C)) and total solute (TS) concentration on the measured freeze-concentration factor (F_{Exp}). Values of F_{FPD} calculated from freezing-point depression are shown as black (–10 ˚C) and gray (–30 ˚C) lines. In panel (B) estimated values of F_{Exp} from Cho et al. for three concentrations of NaCl at –10˚C are also plotted.[9] Colored lines are empirical regression fits to the data, where y = $\log_{10}(F_{Exp})$ and [TS] is in units of mmol/kg: y = (4.3 ± 0.86) $\times 10^3$ for Na_2SO_4 at –10˚C (blue line, which represents the average of the data points with the exception of the lowest value of F_{Exp} at 0.135 mmol/kg TS that was excluded as an outlier), y = –0.041 $(\log_{10}[TS])^2$ – 0.66 $\log_{10}[TS]$ + 3.3 for NaCl at –10˚C (red line), y = –0.041 $(\log_{10}[TS])^2$ – 0.45 $\log_{10}[TS]$ + 3.8 for NaCl at –30˚C (red line), and y = –0.13 $(\log_{10}[TS])^2$ – 0.71 $\log_{10}[TS]$ + 3.3 for $CaCl_2$ at –10˚C (green line).

Figure 4. Ratio of the experimentally measured freeze-concentration factor (F_{Exp}) to the freeze-concentration factor calculated from freezing-point depression (F_{FPD}) over the range of total solute concentrations used in our experiments. Ratios estimated from data in Cho et al.[9] are plotted as crosses for three concentrations of NaCl at –10˚C. A ratio of 1 for F_{Exp}:F_{FPD} indicates perfect agreement of the experiment with the freezing-point depression model. Panel (A) shows results in illuminated ice pellets studied above the eutectic temperatures (T_{eu}) of NaCl and $CaCl_2$, while (B) shows the ratio in pellets studied below T_{eu} of NaCl and Na_2SO_4.

Figure 5. Effect of temperature on measured values of the freeze-concentration factor (F_{Exp}) in illuminated ice pellets containing 6.0 mmol/kg TS as NaCl and 10 nM Rose Bengal (Panel A). Data from the 1.1 mM NaCl solution from Cho et al.[9] is also plotted. The colored line represents values of F_{FPD} calculated from freezing-point depression for total solutes = 6 mmol/kg TS (our conditions) at temperatures above (orange line) and below (red line) the

eutectic temperature of NaCl (−21.5˚C). The thin gray line is F_{FPD} for total solutes = 2.2 mmol/kg TS (conditions of Cho et al.[9]). Panel (B) shows the ratio F_{Exp} to F_{FPD}, with a ratio of 1 indicating perfect agreement between the experiment and freezing-point depression model.

Figures

Figure 1:

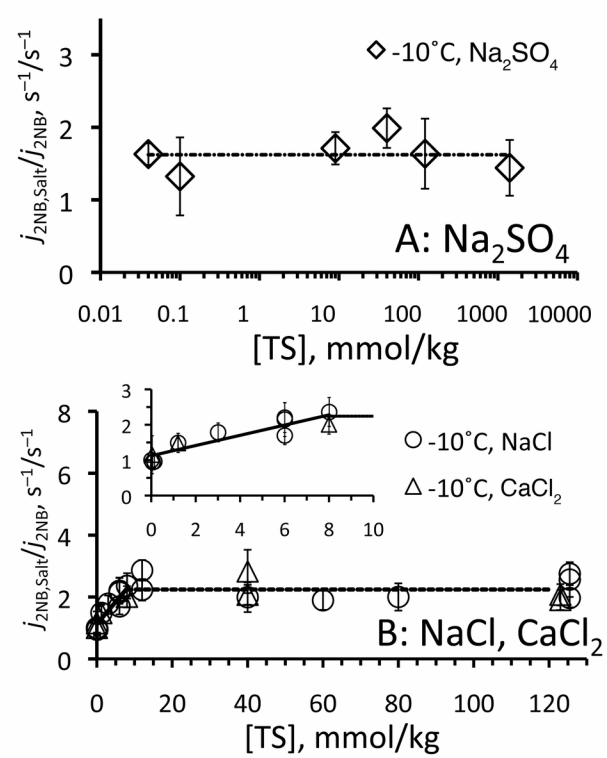

Figure 2:

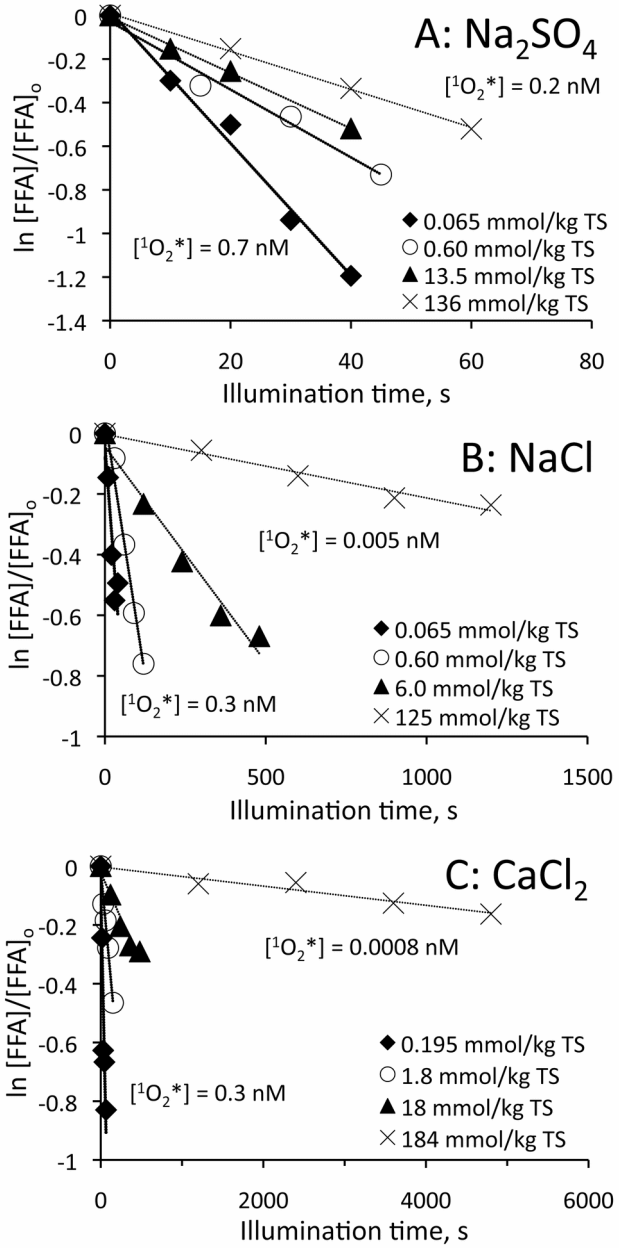
A: Na_2SO_4
$[^1O_2*]$ = 0.2 nM
$[^1O_2*]$ = 0.7 nM
0.065 mmol/kg TS
0.60 mmol/kg TS
13.5 mmol/kg TS
136 mmol/kg TS
ln [FFA]/[FFA]$_o$
Illumination time, s
B: NaCl
$[^1O_2*]$ = 0.005 nM
$[^1O_2*]$ = 0.3 nM
0.065 mmol/kg TS
0.60 mmol/kg TS
6.0 mmol/kg TS
125 mmol/kg TS
C: $CaCl_2$
$[^1O_2*]$ = 0.0008 nM
$[^1O_2*]$ = 0.3 nM
0.195 mmol/kg TS
1.8 mmol/kg TS
18 mmol/kg TS
184 mmol/kg TS

Figure 3:

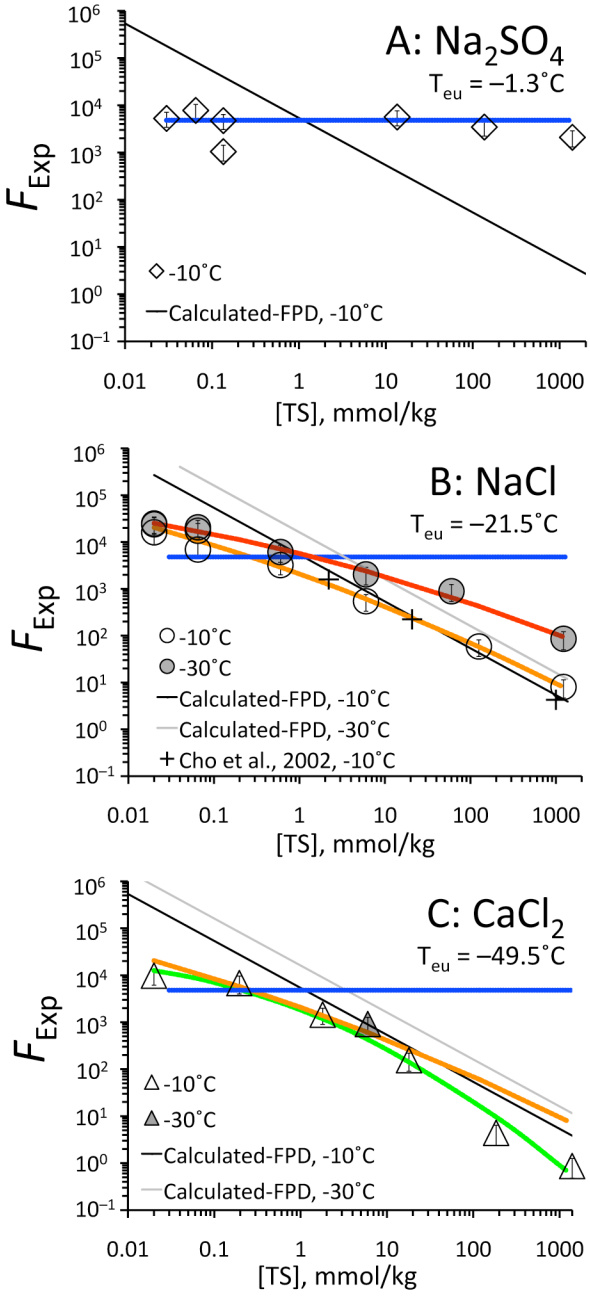
A: Na_2SO_4
T_{eu} = –1.3˚C
F_{Exp}
-10˚C
Calculated-FPD, -10˚C
[TS], mmol/kg
B: NaCl
T_{eu} = –21.5˚C
-10˚C
-30˚C
Calculated-FPD, -10˚C
Calculated-FPD, -30˚C
Cho et al., 2002, -10˚C
C: $CaCl_2$
T_{eu} = –49.5˚C

Figure 4:

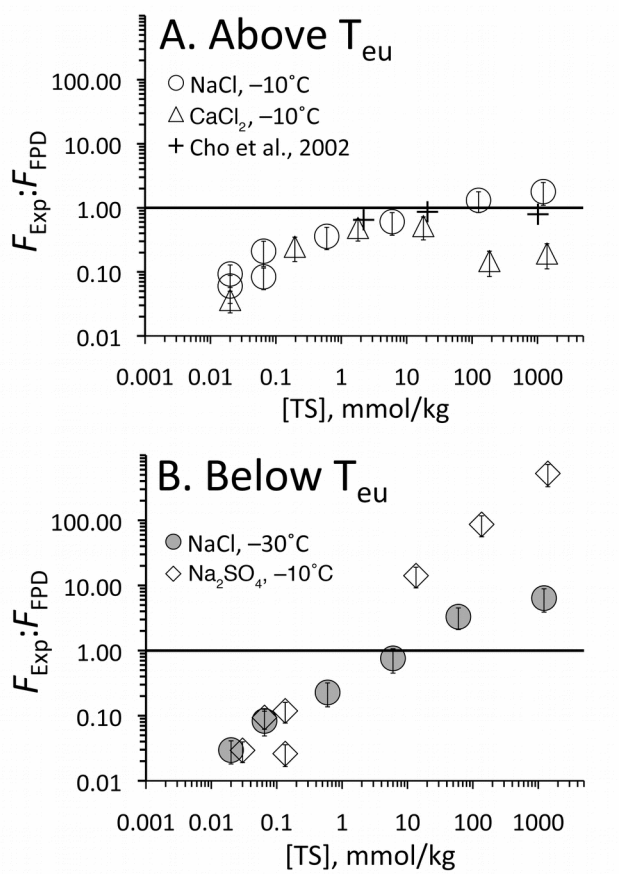
A. Above T_{eu}
NaCl, –10˚C
$CaCl_2$, –10˚C
Cho et al., 2002
$F_{Exp}:F_{FPD}$
100.00
10.00
1.00
0.10
0.01
0.001 0.01 0.1 1 10 100 1000
[TS], mmol/kg
B. Below T_{eu}
NaCl, –30˚C
Na_2SO_4, –10˚C
$F_{Exp}:F_{FPD}$
100.00
10.00
1.00
0.10
0.01
0.001 0.01 0.1 1 10 100 1000
[TS], mmol/kg

Figure 5:

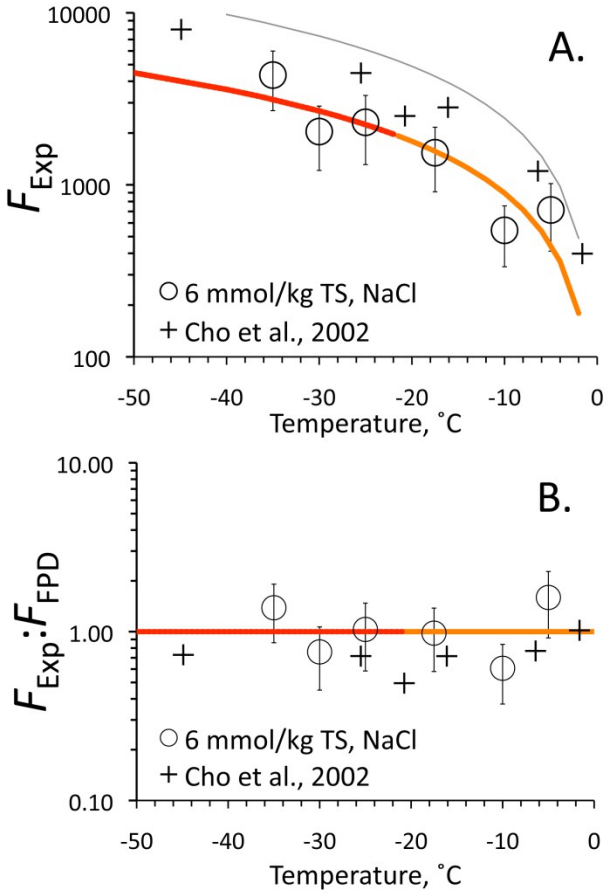
A.
10000
1000
100
F_{Exp}
6 mmol/kg TS, NaCl
Cho et al., 2002
-50
-40
-30
-20
-10
0
Temperature, ˚C
B.
10.00
1.00
0.10
F_{Exp}:F_{FPD}
6 mmol/kg TS, NaCl
Cho et al., 2002
-50
-40
-30
-20
-10
0
Temperature, ˚C

For Table of Contents Only: